Materials and Design 137 (2018) 38–46

Contents lists available at ScienceDirect

Materials and Design

journal homepage: www.elsevier.com/locate/matdes

A facile development of homemade substrate using 'quench free' glass-ceramic composite and printing microstrip patch antenna on it

Pullanchiyodan Abhilash [a,b], Satheesh Babu Roshni [a], Pezholil Mohanan [c], Kuzhichalil P. Surendran [a,b,*]

[a] Materials Science and Technology Division, National Institute for Interdisciplinary Science and Technology (NIIST-CSIR), Thiruvananthapuram 695019, India
[b] Academy of Science and Innovative Research (AcSIR), India
[c] Department of Electronics, Cochin University of Science and Technology, Cochin 682022, Kerala, India

HIGHLIGHTS

- A facile, energy efficient strategy was developed for LTCC substrate applications
- Sintered tapes of non-conventional approach show high resistivity (5.3×10^8 Ω·cm).
- The breakdown strength of sintered tapes comes >1100 V/2 mil.
- A printed antenna operating at 2.5 GHz with a return loss of −19 dB was fabricated.

GRAPHICAL ABSTRACT

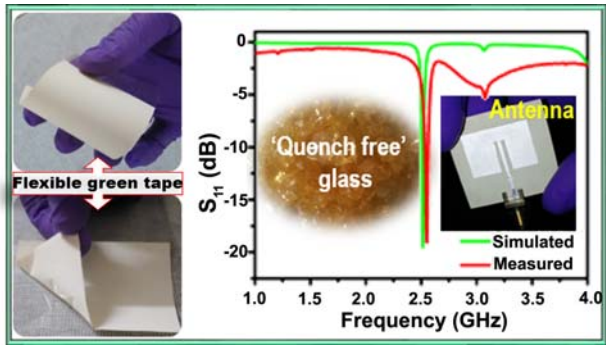

ARTICLE INFO

Article history:
Received 19 July 2017
Received in revised form 6 October 2017
Accepted 6 October 2017
Available online 10 October 2017

Keywords:
LTCC
Glass-ceramics
Dielectric properties
Tape casting
Patch antenna
Microstructure

ABSTRACT

The development of a non-conventional (NC) LTCC glass-ceramic composite using a unique 'quench free glass', and subsequent realization of a patch antenna on this substrate, are reported. This novel composition is comprised of Sr_2ZnTeO_6 (SZT) and 5 wt% of ZBPT (10 mol% ZnO – 2 mol% B_2O_3 – 8 mol% P_2O_5 – 80 mol% TeO_2) glass where the latter reaction mixture can be added directly to the ceramic, bypassing the high temperature melt quenching step. The average particle size distribution shows a more uniform and narrow distribution of powder prepared through non-conventional approach, compared to the conventional approach (C) where the quenched glass powder was added to the ceramic. The sintered tapes show ε_r values of 11.64 and 12.12 for both SZT + ZBPT (C) and SZT + ZBPT (NC) respectively. The breakdown strength of both sintered tapes comes >1100 V/2 mil. The SZT + ZBPT (NC) tape show lower leakage current and better resistivity (5.3×10^8 Ω·cm) compared to SZT + ZBPT (C) (2.9×10^8 Ω·cm). In order to check the feasibility of developed LTCC tape as microwave substrates, a prototype of ceramic patch antenna operating at 2.5 GHz was designed and printed on sintered LTCC tapes of SZT + ZBPT (NC) and its radiation characteristics were analyzed and discussed.

1. Introduction

Recently, the rapid popularization of microelectronic technology, specifically in mobile telecommunication system accelerated the growth of miniaturization of devices [1–3]. Low temperature co-fired ceramic (LTCC) based hybrid technology has larger benefits in this

* Corresponding author at: Materials Science and Technology Division, National Institute for Interdisciplinary Science and Technology (NIIST-CSIR), Thiruvananthapuram 695019, India.
E-mail address: kpsurendran@niist.res.in (K.P. Surendran).

https://doi.org/10.1016/j.matdes.2017.10.015
0264-1275/

scenario. In simple terms, LTCC technology is a multilayer packaging technique, which allows 3D integration of components and interconnections [4–8]. Nowadays, LTCC technology serves as the base for realization of advanced hardware solutions through its multifunctionality, light weight, improved portability and better performance [9–11]. The main attraction of LTCC technology lies in its co-fireability with silver (Ag) at a reduced sintering temperature and chemical inertness with Ag metal [9,12–14]. Major requirement of an LTCC material, apart from its non-reactivity with electrode metals are, low sintering temperature (<960 °C), low dielectric constant (<15), low dielectric loss, high thermal conductivity and low coefficient of thermal expansion (CTE) [4,15–18]. The high volume 3D integration and circuit miniaturization in LTCC technique is possible through multilayer ceramic module (MCM) by stacking of individual green tapes [19]. Hence, the development of defect free uniform green tape with desirable flexibility and plasticity is one of the critical challenges in LTCC technology.

Tape casting process is a well-known cost-effective technique, and is considered as the building block of MCM technology [20,21]. The process begins with the formulation of a viscous slurry composed of ceramic powder with different organic additives like dispersant, plasticizer, binder and homogenizer in the form of a stable colloidal system [1,22,23]. Based on the nature of solvent system used, the tape casting process is generally classified into two categories (*i*) aqueous based (water) and (*ii*) solvent based (organic solvents) [23]. Among the different factors responsible for the stability of dispersion, the main contribution is from the particle size, morphology and surface area of the ceramic powder. Hence, controlling a uniform narrow distribution of particle size and uniform morphology is highly appreciated in tape casting.

For developing LTCC based tapes, one has to ensure that their sintering temperature should be below 900 °C [24]. Among different techniques to reduce the firing temperature of ceramic tapes, the addition of low melting glasses is the cost effective and widely used strategy [25–29]. However, the addition of glasses may react with metal electrode and thereby deteriorate the dielectric properties of the ceramics. Alternatively, the high glass content will make the tape casting process more clumsy and tedious [30,23]. Hence, a lot of research is going on to develop alternative methods and materials for LTCC applications. One of the successful approaches is the use of glass free LTCC materials. Even though there are a lot of glass free LTCC materials available [31–37] only a limited number of reports are there on tape casting of glass free LTCC materials. In 2013, Thomas et al. reported the tape casting process of $LiMgPO_4$ glass free LTCC material having excellent thermal and dielectric properties [23]. In 2015, Abhilash et al. reported the formulation of tape casting slurry of a glass free LTCC material of $Bi_4(SiO_4)_3$ with high solid loading [1]. Earlier, a new and different approach on this aspect was reported by Abhilash et al. in 2013 [6]. In that paper, authors reported a glass composition that can be prepared through a facile slow cooling process and termed it as 'quench free glass' [6]. Further, the paper also discussed about a new strategy developed for LTCC material known as non-conventional method [6]. The present paper is a step ahead of that work where we would like to realize a prototype device out of the ceramic substrate synthesized through non-conventional route.

Microstrip patch antennas (MPA) are increasingly used in modern communication trans receivers, owing to their added advantages like light weight, consistent gain, steady radiation pattern, low cost and compatibility with circuits [38,39]. A MPA usually consists of a thin metallic conductor (commonly silver or copper) and is bonded to a grounded dielectric. The patch antennas radiate due to the fringing fields between the underneath of the patch and the ground plane. When the patch of MPA is excited by a feed, the underneath of the patch is charged to positive and the ground plane is charged to negative and it will create a charge distribution between the ground plane and the underneath of the patch. This, in turn, will result in the patch to radiate due to the fringing fields between the underneath of the metal patch and the ground plane [40].

In order to design compact wireless devices, it is necessary to miniaturize the antenna size accordingly. There are several strategies used for antenna's size reduction. Among them, introduction of high dielectric constant materials as the substrates is most effective for miniaturization in patch antennas [41,42]. However, the use of high dielectric constant material will result in the reduction of band width and radiation efficiency of the developed antenna [41]. Hence, for the practical application, the desired range of dielectric constant suitable for patch antenna fabrication falls within the range 2.2 to 12 [38]. Polymers are unsuitable as substrates for achieving high dielectric constant, while there exist plenty of high dielectric constant ceramic materials. However, the realization of MPAs on ceramic substrate is challenging both from the design as well as practical perspectives. It should be noted that, there are only very few reports on realizing microstrip patch antennas on high dielectric constant hard ceramic substrates. This is primarily because, besides addressing ceramics' inherent narrow bandwidth, the fine machining of the hard substrate and subsequent metallic cladding requires a lot of optimization. One of the most viable solutions is to go for printed antennas, which can minimize the problems of debonding of the radiating patch from the substrate.

In the present paper, we focused on the fabrication of LTCC tapes through an energy efficient approach based on the newly developed non-conventional technique, successfully bypassing high temperature melt quenching process of glass synthesis. Further, the slurry formulation, thermal, structural, dielectric and surface properties of the developed tapes were compared with tapes prepared from conventionally developed composite. The practical utility of the developed LTCC tapes were also evaluated by screen printing a prototype patch antenna on the newly developed LTCC tape.

2. Experimental procedure

2.1. 'Quench free glass'-ceramic composite preparation

A 'quench free glass' having composition 10 mol% ZnO – 2 mol% B_2O_3 – 8 mol% P_2O_5 – 80 mol% TeO_2 (ZBPT) [43,44] and its glass-ceramic composite with Sr_2ZnTeO_6 (SZT) was prepared following our own earlier reports [6]. The average particle size distribution of the powder prepared by both approaches (conventional and non-conventional) was determined by Dynamic Light Scattering (Zetasizer Nanoseries: ZEN 3600, Malvern, Worcestershire, UK). BET surface area of the powder was also measured by nitrogen adsorption using surface area analyzer (Gemini 2375, Micromeritics, Norcross, USA).

2.2. Tape casting

The ceramic composite SZT-5 wt% ZBPT prepared by both conventional and non-conventional approaches were selected as the optimized LTCC composition for tape casting purpose. The composite prepared through conventional and non-conventional approach were designated as SZT + ZBPT (C) and SZT + ZBPT (NC) respectively in the following discussions. The tape casting process for both composites (SZT + ZBPT (C) and SZT + ZBPT (NC)) were carried out using solvent based tape casting technique. A mixture of xylene (Sigma–Aldrich) and ethanol (Merck, Germany) (50:50) was used as solvent. In order to optimize the dispersant amount, we prepared ceramic slurry with varying amount of dispersant, fish oil (Arjuna Natural Extracts, Kerala, India) (0.5–2.0 wt%) with respect to powder. The powder loading was fixed at a constant value of 65 wt% for the dispersant optimization. The viscosity of the slurry was measured by cone and plate method using a rheometer (Rheo plus32, Anton paar, USA), and the sedimentation analysis was carried out in a 5 ml graduated measuring cylinder. The packed bed density of the slurry was investigated from the ratio of the sediment's initial height (H_0) and sediment height (H) after 24 h. Tape casting slip was formulated in two stages, the first stage involves mixing of ceramic powder with optimized dispersant in binary solvent mixture.

In second stage, binder (polyvinyl butyral (PVB), Butvar B-98, Sigma–Aldrich), plasticizers (Butyl benzyl phthalate, Sigma–Aldrich, polyethylene glycol, Sigma–Aldrich), and a homogenizer (cyclohexanone, Sigma–Aldrich) were added [1]. The viscosity of ready-to-cast homogenized slurry was again measured. The LTCC tapes were casted using a tape casting machine (Keko equipment, Zuzemberk, Slovenia) on a silicon coated Mylar® film using the double doctor blade technique [1,23]. The mechanical strength of green tape having sample dimensions of gauge length 40 mm, width 10 mm and thickness 0.10 mm was measured using a Universal Testing Machine (Hounsfield, H5K-S UTM, Redhill, UK) at a crosshead speed of 1 mm/min. To elucidate the binder burnout region the thermogravimetric analysis (TGA) of the green tape was conducted using a thermogravimetric analyzer (PerkinElmer, Waltham, USA). The lamination of individual green tapes were done in isostatic lamination press (Keko equipment, Haikutech, Maastricht, Netherlands) by applying a pressure of 10 MPa and a temperature of 60 °C for 6 min. The laminated tapes were sintered at 900 °C for 6 h, by keeping the laminate in between two porous alumina plates in order to avoid warping. The density of sintered tapes was measured using Archimedes method. Shrinkage of sintered tape in the x (casting direction), y (across the width) and z (across the thickness) direction were measured by the aid of a traveling microscope. Phase purity of the sintered tapes were analyzed using X-ray diffraction analysis (PANalytical X'Pert PRO diffractometer having Nickel filtered Cu Kα, Netherlands). The microstructure of the green and sintered tapes were analyzed using Scanning Electron Microscope (SEM) (JEOL-JSM 5600 LV, Tokyo, Japan). The surface roughness of the green tape was measured using an Atomic Force Microscope (AFM) (Bruker Nano, Inc., USA) operating in the tapping mode regime. The hardness of sintered tapes was measured using Vickers micro indentation hardness test (Shimadzu HMV-2TAW, Kyoto, Japan). The microwave dielectric properties (dielectric constant, ε_r and loss tangent, tanδ) and temperature variation of dielectric constant in the temperature range of 25–60 °C were measured in a Split Post Dielectric Resonator (SPDR) operating at 5 GHz with the aid of a vector network analyzer (Model No. E5071C ENA series, Agilent Technologies, Santa Clara, CA).

2.3. Design and fabrication of microstrip patch antenna

The microstrip patch antenna design was done using Ansoft HFSS (high frequency structure simulator) software. Design parameters are chosen for a center frequency of 2.5 GHz, and the prototype of the antenna were fabricated on sintered SZT + ZBPT (NC) tape of dimensions 30 × 30 × 1.05 mm having a dielectric constant (ε_r) of 11.64 and tanδ of 0.0024. The ground (30 × 30 mm) and patch for the designed antenna were fabricated by screen printing of Ag paste (Metalon® HPS-021LV silver ink) and curing at 400 °C. Antenna is fed by a 50 Ω SMA connector to measure the electrical parameters. A schematic representation of the designed patch antenna along with optimized parameters is represented in Fig. 7. The black labels indicates the dimensions of designed patch and the red labels indicates the positions of the patch along X and Y directions. The fabricated antenna is characterized using Agilent PNA E8362B network analyzer and far-field radiation characteristics were measured in the anechoic chamber.

3. Results and discussion

The particle size distribution (PSD), shape and its orientation have significant influence on green tape properties specifically on shrinkage during sintering [45]. Fig. 1 indicates the PSD of the powder SZT + ZBPT (C) and SZT + ZBPT (NC) respectively.

As evidenced from Fig. 1, SZT + ZBPT (NC) shows narrow distribution of powder with an average particle size of 487 nm. Compared to SZT + ZBPT (NC), the SZT + ZBPT (C) has larger distribution of particle size with an average particle size of 610 nm. This wider distribution of particle size is believed to be contributed from the size and shape

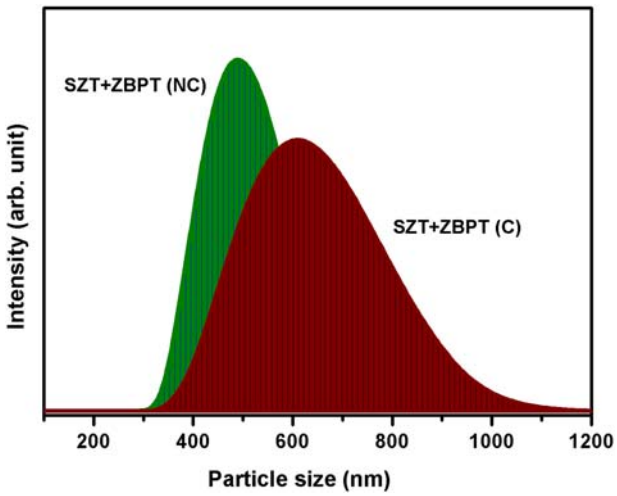

Fig. 1. Particle size distribution of SZT + ZBPT (C) and SZT + ZBPT (NC).

(coarse) of glass powder present in the SZT + ZBPT (C) powder. Higher particle size distribution has a greater influence on the anisotropic shrinkage of tape compared to narrow and uniform distribution of powder [46] (see Table 1). Hence, from the PSD analysis we can infer that, SZT + ZBPT (NC) tapes will have a better control over the shrinkage anisotropy compared to SZT + ZBPT (C) tape. Besides PSD, other main powder characteristic which influence on slurry preparation is specific surface area of the powder since the interaction of organic constituents with powder mainly depends on its surface area. In general, the ideal surface area of the powder suitable for tape casting should fall within the range ~1 to 20 m^2/g [47]. In the present case, BET surface area of the powders SZT + ZBPT (C) and SZT + ZBPT (NC) are comes around 1.5 m^2/g and 1.6 m^2/g respectively.

A stable tape casting slurry requires an optimized amount of dispersant, in order to disperse the primary particles and hold them separately to make the suspension homogeneously throughout the process [47]. The effectiveness of dispersant amount was optimized by viscosity and sedimentation analysis. Fig. 2 (a) and (b) represent the variation in viscosity of the slurries with different dispersant amount (0.5 to 2.0 wt% with respect to powder) of SZT + ZBPT (C) and SZT + ZBPT (NC) respectively. Usually tape casting slurry with better dispersion shows minimum viscosity and slow settling rate with higher pack bed density [48]. From Fig. 2 (a) and (b), we can observe that, as the dispersant amount increases from 0.5 to 1.5 wt%, the viscosity of both slurries (SZT + ZBPT (C) and SZT + ZBPT (NC)) decreases gradually. Whereas, further increase in dispersant amount to 2.0 wt% have no significant influence on viscosity. The decrease in viscosity with dispersant addition is mainly due to the formation of a fluid interparticulate layer between the particles which tend to improve particle mobility. Here, the mechanism involved in suspension's stability is steric stabilization where low dielectric constant organic solvents are used as vehicle. In steric stabilization, one part of the dispersant (fish oil) molecule bond with particle surface, leaving the other part in the solvent. This 'tail' part in the solvent layer hinders particles to joining together, thereby increases the stability of the suspension and lowers the viscosity [47]. One of the assessable effect of using dispersant on stabilizing the suspension in tape casting process is the packed bed density [47]. In order to further investigate the steric stability, 5 ml each of the colloidal suspension with varying amount of dispersant (0.5 to 2.0 wt% fish oil) was added in a graduated measuring cylinder, and the final sediment heights (H) were noted after 24 h. A plot is made for H/H_0 against dispersant concentration and the results are given in Fig. 2 (c) and (d) for SZT + ZBPT (C) and SZT + ZBPT (NC) respectively. It is evident from the figures that, as the dispersant amount increases from 0.5 to 1.5 wt%, the value H/H_0 decreases linearly and reaches its minimum value. Further

Table 1
Microwave dielectric properties and shrinkage (%) of sintered SZT + ZBPT (C) & SZT + ZBPT (NC) tapes.

Material	Thickness (μm)	Relative density (%)	Dielectric properties (5 GHz)		Shrinkage (%)		
			ε_r	tanδ	x	y	z
SZT + ZBPT (C)	392	94	12.12	0.0021	14 ± 2	9 ± 2	7 ± 3
SZT + ZBPT (NC)	382	95	11.64	0.0024	18 ± 2	17 ± 2	7 ± 3

increase in dispersant amount to 2.0 wt% causes a slight increase in H/H_0. A low value of H/H_0 indicates a high packed bed density, which reveals that the suspension having 1.5 wt% of dispersant content has better dispersion stability [48]. Hence, based on the sedimentation analysis, we optimized the dispersant amount to 1.5 wt% with respect to powder for both SZT + ZBPT (C) and SZT + ZBPT (NC) slurries.

The optimized composition of tape casting slurry of both SZT + ZBPT (C) and SZT + ZBPT (NC) is given in Table S1. As stated earlier, the formulation of tape casting slurry involves two stages where the ceramic filler with optimized dispersant is mixed in the first stage while binder, plasticizers etc. were optimized in the second stage. Their optimization is done through trial and error method by inspecting the quality of green tape. Interestingly, the optimized composition of both NC and C tape casting slurries are similar. The maximum powder loading achieved was 60.66% with respect to total composition. The high solid loading attained in tape casting slurry will facilitate the drying speed of the solvent, thereby reduces the drying stress evolved in green tape, which results a crack free microstructure in the dried tape [1,49,50]. The viscosity of optimized slurries is depicted in Fig. 3 (a). It is evident from the figure that viscosity of the ready-to-cast slurry shows typical pseudo plastic behavior, which is one of the prerequisite for an ideally flowing tape casting slurry. This is because, with increase in shear rate, the viscosity decreases that favors smooth flow of slurry through doctor blade. Once the slurry pass over the doctor blade the viscosity will increase, thus it prevents the undesired flow of slurry over the carrier film [23]. The TGA analysis of green tapes were carried out in air atmosphere to a temperature of 1000 °C, aimed to elucidate the thermal degradation of organic constituents used for slurry preparation. Fig. 3 (b) represents the TG curves of both SZT + ZBPT (C) and SZT + ZBPT (NC) green tapes. Both tapes show a very low weight loss (around 1.5%) up to 150 °C, it may be mainly comes from the volatilization of organic solvents used for tape casting. The maximum weight loss occurred in the temperature range of 150 to 450 °C, as shown by the shaded portion. Almost 11% weight loss is happening in this regime which implies that most of the organic additives used in tape casting process decompose in this temperature range. From 450 to 800 °C, the weight loss almost remains constant and thereafter further weight loss occurs. This may be due to the evaporation of low melting glass components present in the tapes. Based on this TGA results, two intermediate binder burnout steps specifically at 300 °C and 600 °C were included in the sintering profile (up to 900 °C) for the complete removal of organic additives. The tapes sintered at 900 °C show complete phase purity without any additional phases, which is evident from the XRD pattern presented in Fig. 3 (c). All the peaks in XRD pattern can be well indexed using standard ICDD file (16-0549) [51]. From the XRD pattern we can further evidence that glass phase used for reducing the sintering temperature in both approaches (conventional and non-conventional) has no apparent reactivity with ceramic powder. Fig. 3 (d) and (e) are the photographic images of the green and sintered tapes of SZT + ZBPT (NC) respectively.

Mechanical strength of green tapes was measured by tensile measurement, using a single layer of green tapes having thickness of ~121 μm and 111 μm for both SZT + ZBPT (C) and SZT + ZBPT (NC)

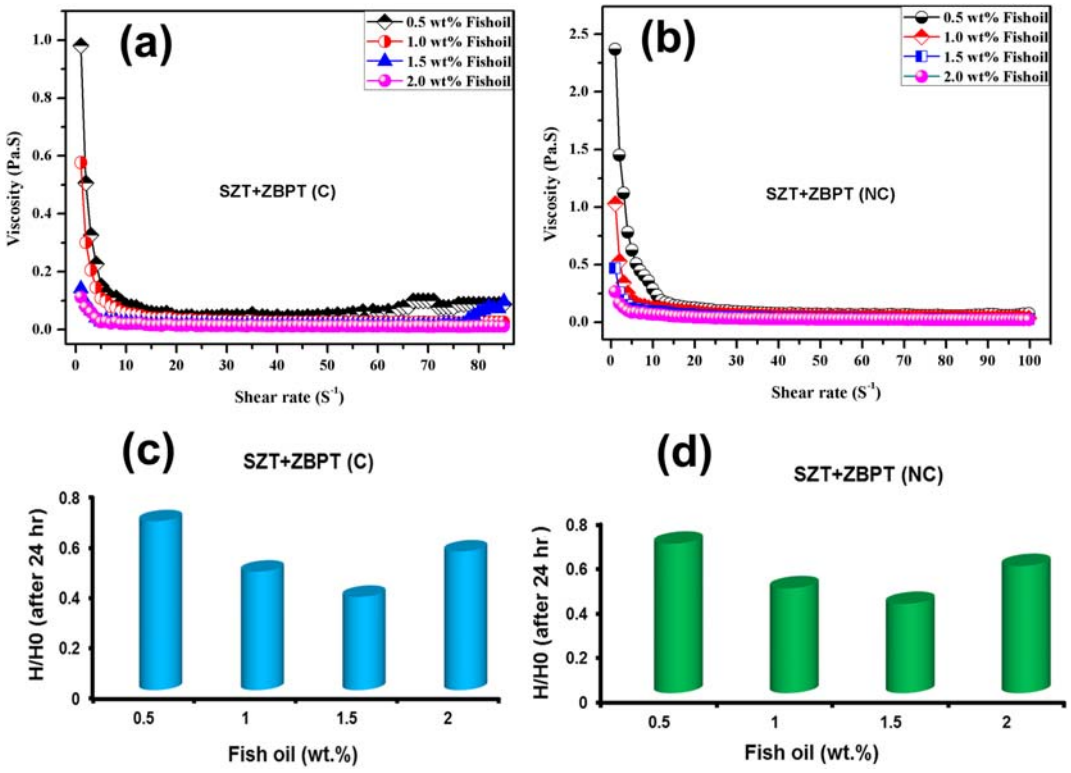

Fig. 2. Variation of viscosity with different wt% of dispersant of (a) SZT + ZBPT (C) and (b) SZT + ZBPT (NC) and packing bed densities with different wt% of dispersant (c) SZT + ZBPT (C) and (d) SZT + ZBPT (NC) respectively.

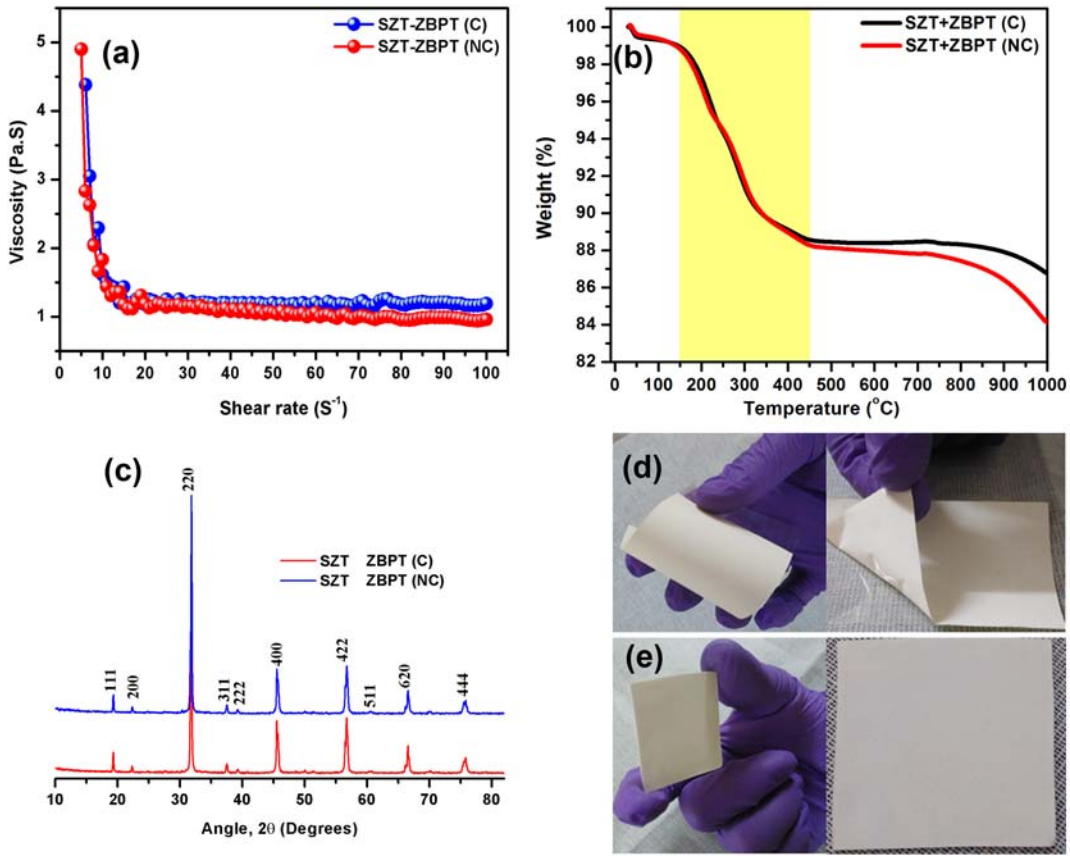

Fig. 3. (a) Viscosity of the optimized tape casting slurry (b) TGA of green tapes (c) XRD pattern of sintered tapes at 900 °C (d) and (e) photographs of green and sintered tapes of SZT + ZBPT (NC).

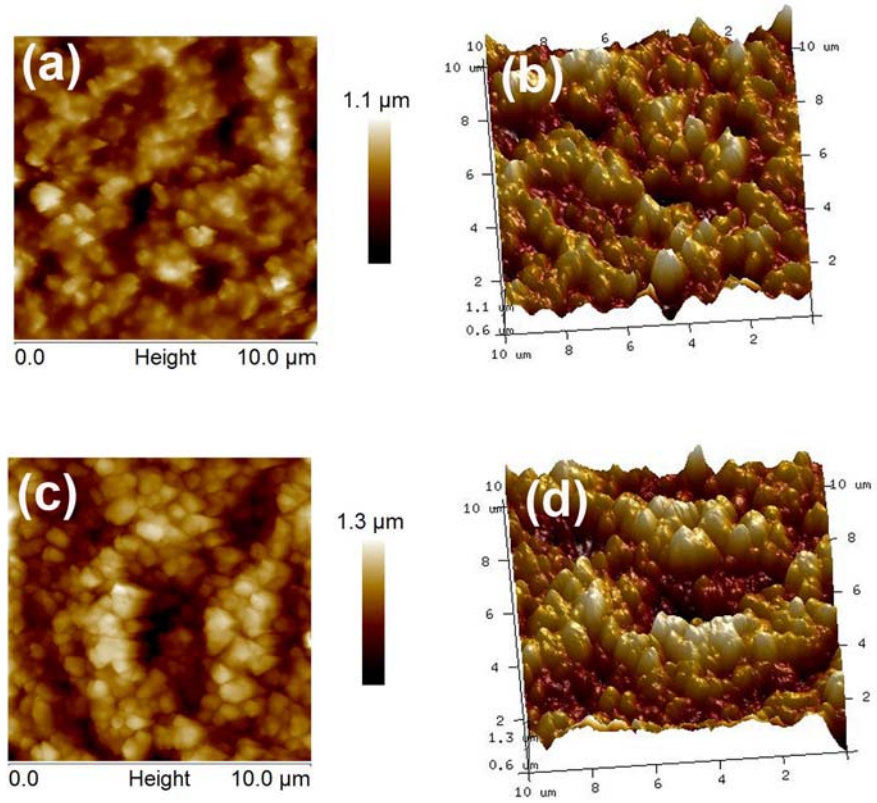

Fig. 4. (a) and (c) 2D AFM images of SZT + ZBPT (C) and SZT + ZBPT (NC), (b) and (d) 3D AFM images of SZT + ZBPT (C) and SZT + ZBPT (NC) respectively.

respectively. The results indicate that single layer of green tapes have tensile strengths of about 0.5 MPa and 0.4 MPa respectively for SZT + ZBPT (C) and SZT + ZBPT (NC), and these value are in good agreement with some of the commercial LTCC tapes and earlier reports [23,1]. Surface roughness plays an important role in printing of conductive patterns and other components in LTCC tapes, where smoother surfaces are not preferred. The AFM results of single layer green tape of both SZT + ZBPT (C) and SZT + ZBPT (NC) is shown in Fig. 4.

Fig. 4 (a) and (c) represent 2D images of SZT + ZBPT (C) and SZT + ZBPT (NC) whereas (b) and (d) indicate 3D images of SZT + ZBPT (C) and SZT + ZBPT (NC) respectively. Average surface roughness (R_a), kurtosis and skewness values of SZT + ZBPT (C) are 116 nm, 3.51, and −0.181 respectively. Since the value of kurtosis is >3 (i.e. 3.51), the surface is believed to has a Gaussian distribution and called as Mesokurtic which indicates that the surface has more peaks than valleys. The negative values of skewness indicate that surface has distribution of longer tails below the reference plane. Similarly for SZT + ZBPT (NC), the average surface roughness (R_a), kurtosis and skewness values are 154 nm, 2.77 and −0.145 respectively. Here the kurtosis values come <3 (i.e. 2.77) indicating the surface to be more flat and be called as Platykurtic. Negative value of skewness here also reveals the presence of longer tailed valley below the reference plane [1,52]. The low average surface roughness of both green tapes assures the uniformity of the surface produced, but not highly smooth, making the printing of functional passive circuits to be rather easy.

More insight into the microstructure of developed tapes can be obtained from SEM images. Fig. 5 (a) and (b) represent the microstructure of green and sintered tape of SZT + ZBPT (C) and Fig. 5 (c) and (d) represent the microstructure of green and sintered tape of SZT + ZBPT (NC) respectively.

From the SEM images of green tape (Fig. 5 (a) and (c)), a more uniformly distributed powder coated with polymer binder can be seen. Porosity comparably lower in the green tape, consequent to the higher powder loading achieved in the first stage of slurry preparation. The sintered microstructure shown in Fig. 5 (b) and (d) reveal the formation of a dense and closely packed microstructure after sintering. The average grain size comes around 1–3 μm for both SZT + ZBPT (C) and SZT + ZBPT (NC) sintered tape.

The mechanical strength of sintered tapes has considerable impact in LTCC technology since the content of glass phases can largely diminishes the mechanical strength of the tape [53]. The micro hardness measurement is versatile tool for getting mechanical strength of sintered body by Vickers hardness test. It is interesting to note that tapes prepared from SZT + ZBPT (NC) show improved hardness value of almost 3.12 ± 0.01 GPa compared to 2 ± 0.01 GPa of SZT + ZBPT (C). The improvement in hardness value for SZT + ZBPT (NC) may be resulted from more homogenized distribution of the glassy phase. The optical micrographs of SZT + ZBPT (C) and SZT + ZBPT (NC) after microindentation is shown in Fig. S1. The impression of the cube cornered diamond tip indent after indentation is highlighted by a dotted circle in the image.

The microwave dielectric properties and percentage shrinkage of sintered tapes of both SZT + ZBPT (C) and SZT + ZBPT (NC) at 5 GHz are given in Table 1. Tapes sintered at 900 °C for 6 h of both SZT + ZBPT (C) and SZT + ZBPT (NC) achieved a maximum densification of ~95%, which is well attested by the SEM micrographs (see Fig. 5 (b) and (d)). Sintered tapes had a ε_r of 12.12 and 11.64 individually for both SZT + ZBPT (C) and SZT + ZBPT (NC) with very low tanδ of the order of 2×10^{-3}. Improvement in dielectric properties of sintered tapes are due to the removal of residual organic components accompanied by grain growth, which favors densification and removal pores. As it evident from the shrinkage data that the SZT + ZBPT (NC) tapes shows a more uniform shrinkage (%) in the x-y direction compared to that of SZT + ZBPT (C), while both tapes have a similar shrinkage (%) in the z-direction. It should be noted that high dielectric constant material as a substrate for a patch antenna have growing interest since it not only reduce the size but also can incorporate directly in monolithic integrated circuits [54]. It also serve to isolate the antenna get affected from nearby things like your hand, your head or by the presence of nearby components (such as cameras, batteries, displays, and speakers) [55]. etc., at the expense of a reduced bandwidth. From this perspective, the newly developed SZT + ZBPT (NC) substrate is advantageous for microstrip patch antenna fabrication.

Dielectric materials cannot resist indefinite amount of voltage. The failure of dielectric materials under the influence of an electric field is commonly known as dielectric breakdown, and it has a major significance in LTCC technology. The measure of dielectric strength which is the minimum electric field required to initiate the dielectric breakdown, will give a clear cut idea about operational stability of the LTCC material. Most of the commercial LTCC substrates like Dupont 951,943, Ferro A6 etc. are reported to possess high dielectric strength. Similarly, the variation of dielectric constant with temperature is another critical factor of

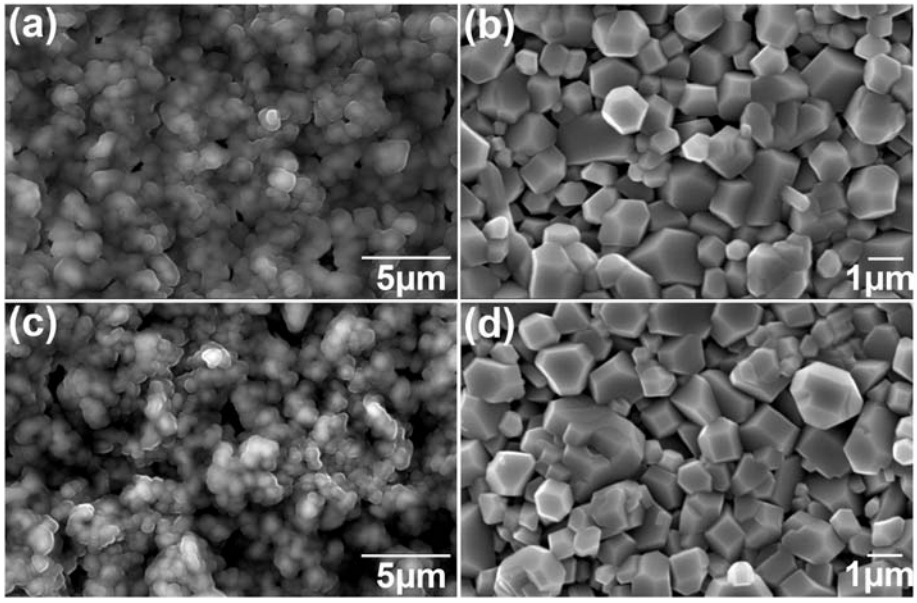

Fig. 5. (a) and (b) SEM images of green and sintered tape of SZT + ZBPT (C), (c) and (d) SEM images of green and sintered tape of SZT + ZBPT (NC) respectively.

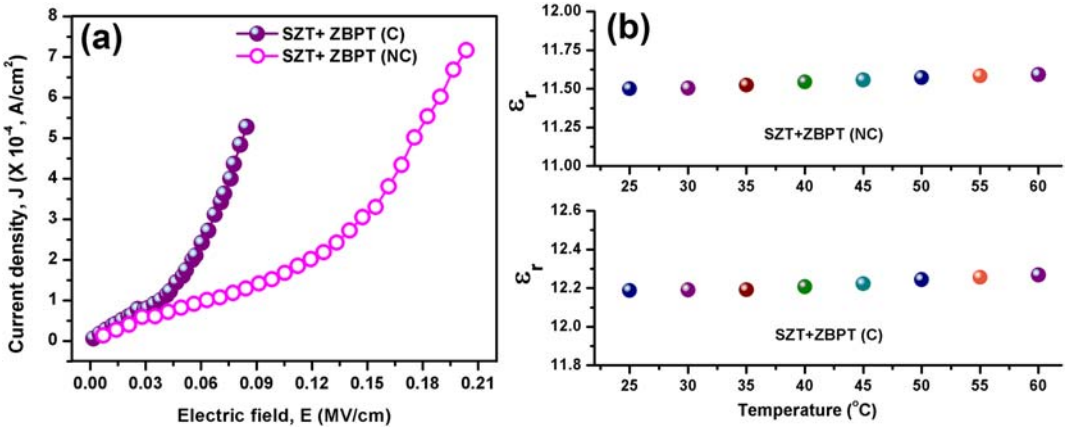

Fig. 6. (a) J-E plot of SZT + ZBPT (C), and SZT + ZBPT (NC) and (b) variation of ε_r with temperature of SZT + ZBPT (C), and SZT + ZBPT (NC) respectively.

practical utility, towards the development of hybrid LTCC devices. In this aspect, we measured current-voltage (I-V) characteristic of the sintered tapes having a thickness of around 2 mil (50 μm) in a voltage range of 1100 V. Typical current density vs. electric field (J-E) plots are shown in Fig. 6 (a). It is evident from the figure that both samples (SZT + ZBPT (C) and SZT + ZBPT (NC)) show specific dielectric nature, where the current density permeable through the sample is very low, of the order of 10^{-4} A/cm^2. Moreover, both samples doesn't undergo a dielectric breakdown even at the maximum voltage applied. Hence, it is logical to believe that the dielectric breakdown strength of both composite will be >1100 V/2 mil. Besides, SZT + ZBPT (NC) tape show lower leakage current and better resistivity ($5.3 \times 10^8\ \Omega \cdot$cm) compared

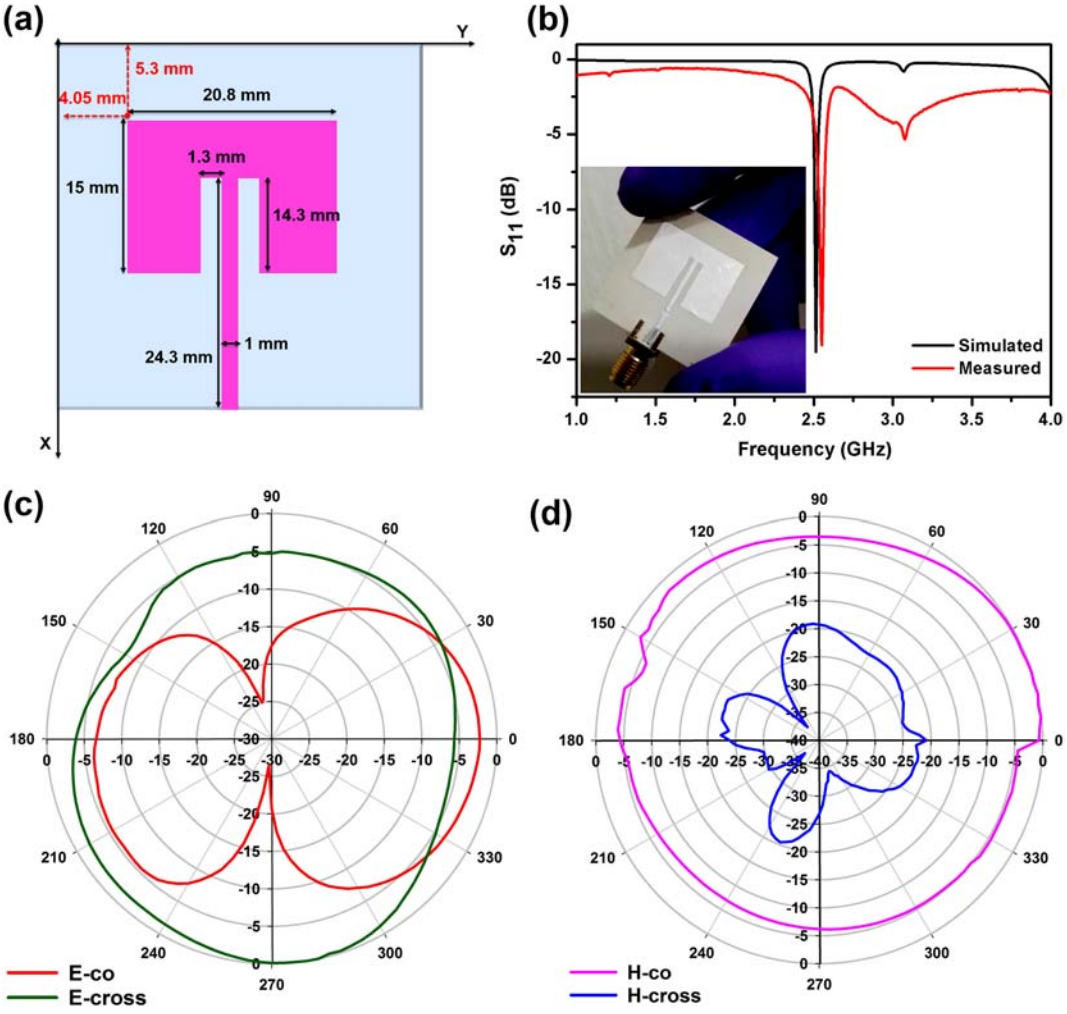

Fig. 7. (a) Schematics of the designed patch antenna (b) return loss (S_{11}) of measured and simulated patch antenna with photograph of the fabricated antenna (inset), (c) and (d) measured radiation pattern of patch antenna along E-plane and H-plane respectively.

to that of SZT + ZBPT (C) which have a resistivity of (2.9×10^8 Ω·cm). The variation in ε_r with ambient temperature for SZT + ZBPT (C) and SZT + ZBPT (NC) were shown in Fig. 6 (b). The results indicate that ε_r varies almost linearly with temperature for both samples.

Finally, in order to check the practical aptness of the SZT + ZBPT (NC) based LTCC substrate, a prototype of patch antenna operating at 2.5 GHz was designed, fabricated and tested with the aid of an Agilent PNA E8362B network analyzer. This kind of patch antennas radiating at 2.5 GHz are ideal to be used in Long-Term Evolution (LTE) handsets which is a standard for high-speed wireless communication band for mobile phones and data terminals. Schematic representation of simulated patch antenna was shown in Fig. 7 (a). The simulated and measured return loss (S_{11}) of the fabricated antenna are depicted in Fig. 7 (b). As it evident from the figure, fabricated patch antenna shows a return loss of around −19 dB and is well matched with simulation results. It should be noted that the simulated resonant frequency of the antenna is 2.51 GHz while that of the measured is 2.55 GHz. A marginal disagreement between simulated and experimental radiating frequency is permissible which is mainly due to the influence of the connector. Further, it should be noted that minute variations in the machined antenna dimensions, surface uniformity of the printed radiating pattern and even geographical inhomogeneities in the dielectric properties of the ceramic substrate etc. can alter the radiation characteristics of such antennas. Photograph of the printed ceramic patch antenna is shown in the inset of Fig. 7 (b). Normalized 2-dimensional radiation patterns along E-plane and H-plane are also shown in Fig. 7 (c) and (d) respectively. The radiation pattern of proposed antenna exhibits similar characteristics of standard rectangular patch and shows linear polarization [56].

4. Conclusions

A facile model to synthesize glass ceramic composites and their subsequent use as a low loss, low firing substrate for printed patch antenna is described in this paper. 'Quench free glass' ceramic slurry and their crack free tapes were developed for LTCC applications. The structural, microstructural, mechanical and dielectric properties of the developed green and sintered tapes were investigated using the non-conventional method and compared with those developed from conventionally prepared composites. Interestingly, the novel method yielded tapes with more uniform and narrower microstructures. Further, micro hardness analysis of sintered tape showed an improved value of 3.12 ± 0.01 GPa for SZT + ZBPT (NC) compared to 2 ± 0.01 GPa of SZT + ZBPT (C), indicating a more homogenized distribution of glass phase in 'quench free glass' composite. The microwave dielectric properties of tapes synthesized through the non-conventional method that were sintered at 900 °C up to a densification of 95%, showed an ε_r of 11.64 and a tanδ of 0.0024 at 5 GHz.

For the realization of compact wireless devices, judicial selection of high dielectric constant substrate that can miniaturize size of the antenna, is necessary. The present material, SZT + ZBPT (NC), is an ideal choice for hard ceramic substrate applications due to its interesting dielectric properties. A prototype of micro strip path antenna operating at 2.5 GHz was designed and fabricated on an accurately machined sintered LTCC tape based on SZT + ZBPT (NC) by creating patch and ground through flatbed screen printing technique. The radiation parameters of the newly designed ceramic antenna showed very good agreement between simulated and measured results, reiterating the efficacy of the new method to develop microelectronic and microwave communication substrates.

Acknowledgements

The authors acknowledge the Technology System Development programme of Department of Science and Technology (ref: DST/TSG/AMT/2015/359), New Delhi for financial assistance. One of the authors P. Abhilash thanks Council of Scientific and Industrial Research, New Delhi for his research fellowship.

Appendix A. Supplementary data

Supplementary data to this article can be found online at https://doi.org/10.1016/j.matdes.2017.10.015.

References

[1] P. Abhilash, M.T. Sebastian, K.P. Surendran, Glass free, non-aqueous LTCC tapes of $Bi_4(SiO_4)_3$ with high solid loading, J. Eur. Ceram. Soc. 35 (2015) 2313–2320, https://doi.org/10.1016/j.jeurceramsoc.2015.02.002.
[2] P. Abhilash, M.T. Sebastian, K.P. Surendran, Structural, thermal and dielectric properties of rare earth substituted eulytite for LTCC applications, J. Eur. Ceram. Soc. 36 (2016) 1939–1944, https://doi.org/10.1016/j.jeurceramsoc.2016.02.019.
[3] Y. Wang, R. Zuo, C. Zhang, J. Zhang, T. Zhang, Low-temperature-fired $ReVO_4$ (Re = La, Ce) microwave dielectric ceramics, J. Am. Ceram. Soc. 98 (2015) 1–4, https://doi.org/10.1111/jace.13378.
[4] J.J. Bian, Q. Yu, J.J. He, Tape casting and characterization of $Li_{2.08}TiO_3$-LiF glass free LTCC for microwave applications, J. Eur. Ceram. Soc. 37 (2017) 647–653, https://doi.org/10.1016/j.jeurceramsoc.2016.09.022.
[5] A. Mohanram, G.L. Messing, D.J. Green, Densification and sintering viscosity of low-temperature co-fired ceramics, J. Am. Ceram. Soc. 88 (2005) 2681–2689, https://doi.org/10.1111/j.1551-2916.2005.00497.x.
[6] P. Abhilash, D. Thomas, K.P. Surendran, M.T. Sebastian, Facile synthesis of "quench-free glass" and ceramic-glass composite for LTCC applications, J. Am. Ceram. Soc. 96 (2013) 1533–1537, https://doi.org/10.1111/jace.12209.
[7] N. Joseph, J. Varghese, T. Siponkoski, M. Teirikangas, M.T. Sebastian, H. Jantunen, Glass-free $CuMoO_4$ ceramic with excellent dielectric and thermal properties for ultralow temperature cofired ceramic applications, ACS Sustain. Chem. Eng. 4 (2016) 5632–5639, https://doi.org/10.1021/acssuschemeng.6b01537.
[8] M.T. Sebastian, Dielectric Materials for Wireless Communication, First, Elsevier, Amsterdam, 2008.
[9] A. Bittner, H. Seidel, U. Schmid, High-frequency characterization of porous low-temperature cofired ceramics substrates, J. Am. Ceram. Soc. 93 (2010) 3778–3781, https://doi.org/10.1111/j.1551-2916.2010.03928.x.
[10] H.-I. Hsiang, B.J. Lyu, L.-T. Mei, C.-S. Hsi, Ag precipitation at the free interface of multilayer NiCuZn ferrites/LTCC components, J. Eur. Ceram. Soc. 36 (2016) 1191–1195, https://doi.org/10.1016/j.jeurceramsoc.2015.12.002.
[11] H. Birol, T. Maeder, P. Ryser, Application of graphite-based sacrificial layers for fabrication of LTCC (low temperature co-fired ceramic) membranes and microchannels, J. Micromech. Microeng. 17 (2006) 50–60, https://doi.org/10.1088/0960-1317/17/1/007.
[12] I.J. Induja, P. Abhilash, S. Arun, K.P. Surendran, M.T. Sebastian, LTCC tapes based on Al_2O_3-BBSZ glass with improved thermal conductivity, Ceram. Int. 41 (2015) 13572–13581, https://doi.org/10.1016/j.ceramint.2015.07.152.
[13] S.X. Dai, Localized temperature stability in low-temperature cofired ceramics, J. Am. Ceram. Soc. 96 (2013) 2499–2505, https://doi.org/10.1111/jace.12347.
[14] J.-S. Kim, N.-H. Nguyen, M.-E. Song, J.-B. Lim, D.-S. Paik, S. Nahm, J.-H. Paik, B.-H. Choi, S.-J. Yu, Effect of Bi_2O_3 addition on the sintering temperature and microwave dielectric properties of Zn_2SiO_4 ceramics, Int. J. Appl. Ceram. Technol. 6 (2009) 581–586, https://doi.org/10.1111/j.1744-7402.2008.02335.x.
[15] M.T. Sebastian, H. Jantunen, Low loss dielectric materials for LTCC applications: a review, Int. Mater. Rev. 53 (2008) 57–90, https://doi.org/10.1179/174328008X277524.
[16] J. Varghese, S. Gopinath, M.T. Sebastian, Effect of glass fillers in $Cu_2ZnNb_2O_8$ ceramics for advanced microwave applications, Mater. Chem. Phys. 137 (2013) 811–815, https://doi.org/10.1016/j.matchemphys.2012.10.014.
[17] M.T. Sebastian, R. Ubic, H. Jantunen, Low-loss dielectric ceramic materials and their properties, Int. Mater. Rev. 60 (2015) 392–412, https://doi.org/10.1179/1743280415Y.0000000007.
[18] M.T. Sebastian, H. Wang, H. Jantunen, Low temperature co-fired ceramics with ultra-low sintering temperature: a review, Curr. Opin. Solid State Mater. Sci. 20 (2016) 151–170, https://doi.org/10.1016/j.cossms.2016.02.004.
[19] A.E. Gurdal, S. Tuncdemir, K. Uchino, C.A. Randall, Low temperature co-fired multilayer piezoelectric transformers for high power applications, Mater. Des. 132 (2017) 512–517, https://doi.org/10.1016/j.matdes.2017.07.030.
[20] S. Le, K.N. Sun, N. Zhang, X. Zhu, H. Sun, Y.X. Yuan, X. Zhou, Fabrication and evaluation of anode and thin Y_2O_3-stabilized ZrO_2 film by co-tape casting and co-firing technique, J. Power Sources 195 (2010) 2644–2648, https://doi.org/10.1016/j.jpowsour.2009.11.039.
[21] S. Chao, F. Dogan, Processing and dielectric properties of TiO_2 thick films for high-energy density capacitor applications, Int. J. Appl. Ceram. Technol. 8 (2011) 1363–1373, https://doi.org/10.1111/j.1744-7402.2010.02592.x.
[22] Z. Jingxian, J. Dongliang, L. Weisensel, P. Greil, Deflocculants for tape casting of TiO_2 slurries, J. Eur. Ceram. Soc. 24 (2004) 2259–2265, https://doi.org/10.1016/S0955-2219(03)00636-8.
[23] D. Thomas, P. Abhilash, M.T. Sebastian, Casting and characterization of $LiMgPO_4$ glass free LTCC tape for microwave applications, J. Eur. Ceram. Soc. 33 (2013) 87–93, https://doi.org/10.1016/j.jeurceramsoc.2012.08.002.
[24] S. Rajesh, H. Jantunen, M. Letz, S. Pichler-Willhelm, Low temperature sintering and dielectric properties of alumina-filled glass composites for LTCC applications, Int. J. Appl. Ceram. Technol. 9 (2012) 52–59, https://doi.org/10.1111/j.1744-7402.2011.02684.x.
[25] K. Makarovič, A. Meden, M. Hrovat, J. Holc, A. Benčan, A. Dakskobler, M. Kosec, The effect of processing conditions on the properties of LTCC material, J. Am. Ceram. Soc. 95 (2012) 760–767, https://doi.org/10.1111/j.1551-2916.2011.05027.x.

[26] M.A. Sanoj, M.R. Varma, Sinterability and microwave dielectric properties of $0.95MgTiO_3$–$0.05CaTiO_3$–glass ceramic composites, J. Alloys Compd. 477 (2009) 565–569, https://doi.org/10.1016/j.jallcom.2008.10.069.
[27] J. Varghese, T. Siponkoski, M. Teirikangas, M.T. Sebastian, A. Uusimaki, H. Jantunen, Structural, dielectric, and thermal properties of Pb free molybdate based ultralow temperature glass, ACS Sustain. Chem. Eng. 4 (2016) 3897–3904, https://doi.org/10.1021/acssuschemeng.6b00721.
[28] X. Du, H. Su, H. Zhang, Z. Zhou, Y. Jing, G. Gan, X. Tang, High-Q microwave dielectric properties of $Li(Zn_{0.95}Co_{0.05})_{1.5}SiO_4$ ceramics for LTCC applications, Ceram. Int. 43 (2017) 7636–7640, https://doi.org/10.1016/j.ceramint.2017.03.058.
[29] H. Zuo, X. Tang, H. Zhang, Y. Lai, Y. Jing, H. Su, Low-dielectric-constant $LiAlO_2$ ceramics combined with LBSCA glass for LTCC applications, Ceram. Int. 43 (2017) 8951–8955, https://doi.org/10.1016/j.ceramint.2017.04.034.
[30] H. Jantunen, R. Rautioaho, A. Uusimäki, S. Leppävuori, Preparing low-loss low-temperature cofired ceramic material without glass addition, J. Am. Ceram. Soc. 83 (2004) 2855–2857, https://doi.org/10.1111/j.1151-2916.2000.tb01644.x.
[31] J. Bian, D.-W. Kim, K.S. Hong, Glass-free LTCC microwave dielectric ceramics, Mater. Res. Bull. 40 (2005) 2120–2129, https://doi.org/10.1016/j.materresbull.2005.07.003.
[32] D. Thomas, M.T. Sebastian, Temperature-compensated $LiMgPO_4$: a new glass-free low-temperature cofired ceramic, J. Am. Ceram. Soc. 93 (2010) 3828–3831, https://doi.org/10.1111/j.1551-2916.2010.03934.x.
[33] N.X. Wu, J.J. Bian, Glass-free low-temperature co-fired ceramics microwave ceramic $AW_{1-x}TexO_4$ (A = Ca, Sr, Zn), Int. J. Appl. Ceram. Technol. 8 (2011) 1494–1500, https://doi.org/10.1111/j.1744-7402.2011.02611.x.
[34] C.-F. Tseng, P.-A. Lin, Microwave dielectric properties of novel glass-free low-firing Li_2CeO_3 ceramics, J. Am. Ceram. Soc. 97 (2014) 1020–1022, https://doi.org/10.1111/jace.12880.
[35] G. Subodh, M.T. Sebastian, Glass-free $Zn_2Te_3O_8$ microwave ceramic for LTCC applications, J. Am. Ceram. Soc. 90 (2007) 2266–2268, https://doi.org/10.1111/j.1551-2916.2007.01673.x.
[36] L. Pang, W. Liu, D. Zhou, Z.-X. Yue, Novel glass-free low-temperature fired microwave dielectric ceramics: $Bi(Ga_{1/3}Mo_{2/3})O_4$, Ceram. Int. 42 (2016) 4574–4577, https://doi.org/10.1016/j.ceramint.2015.11.152.
[37] J.J. Bian, L. Wang, Glass-free LTCC microwave ceramic-$(La_{0.5}Na_{0.5})_{1-x}(Li_{0.5}Nd_{0.5})_xWO_4$, J. Am. Ceram. Soc. 94 (2011) 3188–3191, https://doi.org/10.1111/j.1551-2916.2011.04757.x.
[38] K.V. Rop, D.B.O. Konditi, Performance analysis of a rectangular microstrip patch antenna on different dielectric substrates, Innov. Syst. Des. Eng. 3 (2012) 7–15.
[39] F. Xu, Y. Qiu, Simulation and electromagnetic performance of cylindrical two-element microstrip antenna array integrated in 3D woven glass fiber/epoxy composites, Mater. Des. 89 (2016) 1048–1056, https://doi.org/10.1016/j.matdes.2015.10.091.
[40] D. Bhalla, K. Bansal, Design of a rectangular microstrip patch antenna using inset feed technique, IOSR J. Electron. Commun. Eng. 7 (2013) 8–13.
[41] G.-M. Yang, O. Obi, M. Liu, N.X. Sun, Miniaturized patch antennas with ferrite/dielectric/ferrite magnetodielectric sandwich substrate, Prog. Electromagn. Res. Symp. Proc. 2011, pp. 903–906.
[42] T. Prodromakis, C. Papavassiliou, Towards a microstrip antenna on synthetic high-dielectric substrates, Tenth High Freq. Postgrad. Student Colloq. 5 2005, pp. 57–61.
[43] P. Mošner, K. Vosejpková, L. Koudelka, L. Montagne, B. Revel, Structure and properties of ZnO–B_2O_3–P_2O_5–TeO_2 glasses, Mater. Chem. Phys. 124 (2010) 732–737, https://doi.org/10.1016/j.matchemphys.2010.07.048.
[44] P. Mošner, K. Vosejpková, L. Koudelka, L. Beneš, Thermal studies of ZnO–B_2O_3–P_2O_5–TeO_2 glasses, J. Therm. Anal. Calorim. 107 (2011) 1129–1135, https://doi.org/10.1007/s10973-011-1535-4.
[45] A. Heunisch, A. Dellert, A. Roosen, Effect of powder, binder and process parameters on anisotropic shrinkage in tape cast ceramic products, J. Eur. Ceram. Soc. 30 (2010) 3397–3406, https://doi.org/10.1016/j.jeurceramsoc.2010.08.012.
[46] G. Besendörfer, A. Roosen, Particle shape and size effects on anisotropic shrinkage in tape-cast ceramic layers, J. Am. Ceram. Soc. 91 (2008) 2514–2520, https://doi.org/10.1111/j.1551-2916.2008.02510.x.
[47] R.E.Mistler and E.R.Twiname, Tape casting: theory and practice. OH, USA: The American Ceramic Society; 2000, (n.d.). http://www.amazon.com/Tape-Casting-Practice-Richard-Mistler/dp/1574980297 (accessed August 1, 2014).
[48] N.P. Prasanth, J.M. Varghese, K. Prasad, B. Krishnan, a. Seema, K.R. Dayas, Tape casting of nickel manganite NTC ceramics for chip thermistors, J. Mater. Sci. Mater. Electron. 19 (2007) 1100–1104, https://doi.org/10.1007/s10854-007-9475-2.
[49] A. Seal, D. Chattopadhyay, A. Das Sharma, A. Sen, H.S. Maiti, Influence of ambient temperature on the rheological properties of alumina tape casting slurry, J. Eur. Ceram. Soc. 24 (2004) 2275–2283, https://doi.org/10.1016/j.jeurceramsoc.2003.08.002.
[50] J. Gurauskis, C. Baudín, a.J. Sánchez-Herencia, Tape casting of Y-TZP with low binder content, Ceram. Int. 33 (2007) 1099–1103, https://doi.org/10.1016/j.ceramint.2006.03.014.
[51] A. Dias, G. Subodh, M.T. Sebastian, R.L. Moreira, Vibrational spectroscopic study of Sr_2ZnTeO_6 double perovskites, J. Raman Spectrosc. 41 (2009) 702–706, https://doi.org/10.1002/jrs.2494.
[52] A. Pullanchiyodan, K.P. Surendran, Formulation of sol–gel derived bismuth silicate dielectric ink for flexible electronics applications, Ind. Eng. Chem. Res. 55 (2016) 7108–7115, https://doi.org/10.1021/acs.iecr.6b00871.
[53] S. Arun, M.T. Sebastian, K.P. Surendran, $Li_2ZnTi_3O_8$ based high κ LTCC tapes for improved thermal management in hybrid circuit applications, Ceram. Int. (2017)https://doi.org/10.1016/j.ceramint.2017.01.073.
[54] J.S. Colburn, Patch antennas on externally perforated high dielectric constant substrates, IEEE Trans. Antennas Propag. 47 (1999) 1785–1794, https://doi.org/10.1109/8.817654.
[55] J. Anguera, A. Andújar, M.C. Huynh, C. Orlenius, C. Picher, C. Puente, Advances in antenna technology for wireless handheld devices, Int. J. Antennas Propag. 2013 (2013) 1–25, https://doi.org/10.1155/2013/838364.
[56] M. Islam, M. Islam, M. Samsuzzaman, M. Faruque, N. Misran, A negative index metamaterial-inspired UWB antenna with an integration of complementary SRR and CLS unit cells for microwave imaging sensor applications, Sensors 15 (2015) 11601–11627, https://doi.org/10.3390/s150511601.